Effects of spatial diffusion on nonequilibrium steady states in a model for prebiotic evolution

B. F. Intoy, A. Wynveen, and J. W. Halley*
School of Physics and Astronomy, University of Minnesota, Minneapolis, Minneapolis 55455, USA
(Received 15 June 2016; revised manuscript received 19 September 2016; published 28 October 2016)

Effects of spatial diffusion in a Kauffman-like model for prebiotic evolution previously studied in a "well-mixed" limit are reported. The previous model was parametrized by a parameter p defined as the probability that a possible reaction in a network of reactions characterizing the artificial chemistry actually appears in the chemical network. In the model reported here, we numerically study a grid of such well-mixed reactors on a two-dimensional spatial lattice in which the model chemical constituents can hop between neighboring reactors at a rate controlled by a second parameter η. We report the frequency of appearance of three distinct types of nonequilibrium steady states, characterized as "diffusively alive locally dead" (DALD), "diffusively dead locally alive" (DDLA) and "diffusively alive locally alive" (DALA). The types are defined according to whether they are chemically equilibrated at each site, diffusively equilibrated between sites, or neither, respectively. With our parametrization of the definitions of these nonequilibrium states, many of the DALA states are growing rapidly in population due to the explosive population growth of a few sites, while their entropy remains well below its equilibrium value. Sharp temporal transitions occur as exploding sites appear. DALD states occur less commonly than the other types and also usually harbor a few explosively growing sites but transitions are less sharp than in DALA systems.

DOI: 10.1103/PhysRevE.94.042424

I. INTRODUCTION

In many models and discussions of prebiotic evolution, spatial considerations play a central role. The reason is that the processes that might result in nonequilibrium (lifelike) states, however defined, tend to be fragile and susceptible to decay to equilibrium by various kinds of perturbation. Spatial isolation from perturbations is often invoked as a mechanism by which such decay might be avoided [1,2]. Spatial isolation is often similarly invoked as a way of protecting nonequilibrium metastable behavior from decay to equilibrium at later stages of evolution [3].

However, in studies of a model of prebiotic evolution on which we previously reported [4], the artificial chemical system was assumed to be "well mixed" so that every molecule could react with every other one, as it is in many similar models [5], and explicit effects of any spatial heterogeneity were ignored. When metastable "lifelike" states occurred in that model, they were protected from decay to equilibrium by bottlenecks in the dynamics of these states due to the sparseness of the network of chemical reactions without any explicit reference to space.

We did find that metastable nonequilibrium states occurred in that model, as long as the network of chemical reactions was sufficiently sparse to block decay to equilibrium, but sufficiently connected to allow growth of the molecular ensemble out to the maximum allowed lengths. The sparseness of the chemical network was characterized by a parameter p (the probability that a chemical reaction from a list of all possible reactions is included in the chemical network) and, in terms of it, the probability of occurrence of lifelike states had a maximum at a small finite value of p.

Here we report results of simulations of an extension of that model which allows the possibility of the diffusion of the (artificial) chemical constituents on a spatial lattice. We place copies of our previous model on the vertices of a two-dimensional lattice and allow molecules to hop between these "islands" (or perhaps "cells") at a rate controlled by a second parameter η. There are two implicit time scales in such a model: one characterizing intraisland reactions (controlled by p) and the other characterizing the diffusion between islands (controlled by η). As a physical realization one might imagine a heterogeneous mineral surface on which reacting regions are separated by diffusion barriers.

We address the question of the effects of the presence of this type of diffusion on the likelihood of appearance, and possibly growth and evolution, of lifelike states as studied earlier in the absence of diffusion. In the previous study, we characterized a steady-state system as lifelike under the condition that it was out of chemical equilibrium and had dynamic internal chemistry. In the model studied here we explore three kinds of nonequilibrium steady states which are respectively out of diffusive equilibrium but in chemical equilibrium within each island [diffusively alive and locally dead (DALD)], in diffusive equilibrium but out of equilibrium on each island [diffusively dead and locally alive (DDLA)], or out of equilibrium in both respects [diffusively alive and locally alive (DALA)]. All are found to occasionally occur with measurable frequency in the model in different regions of the p-η plane.

In the next section we describe our previous model and its extension to a system consisting of a two-dimensional lattice of islands or local sites. Population dynamics with identical chemical networks are simulated, as in our previous model, on each site, but now diffusion may occur between these sites. (In the rest of the paper we will use the terms "islands" and "sites" interchangeably to refer to the same entities in the model.) Sections III and IV summarize the entropic criteria used to distinguish the three kinds of nonequilibrium (that is lifelike) states. Sections V and VI present results followed by a discussion and conclusions.

II. MODEL

As in our previous work [4], and following [5–7], the entities which we call "polymers" or, equivalently, "molecules"

*Corresponding author: halle001@umn.edu

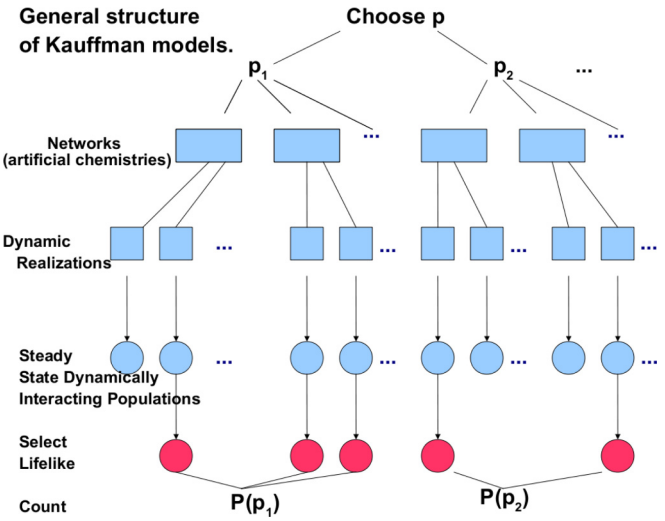

FIG. 1. Structure of the model implementation for a single site.

in the model are strings of 0's and 1's which abstractly represent polymers built from two types of monomers. Further discussion of this choice appears in [4]. A qualitative "road map" of the computations which we carry out in all the Kauffman-like models which we have been studying for a single site is shown in Fig. 1. Given model parameters, namely p for the single-island model of Ref. [4] and p and η for the model studied here, we first generate a large ensemble of "artificial chemistries" numerically. The chemical constituents or species that are modeled as binary polymer strings may, in the model, undergo ligation and scission. The parameter p is the probability that, of all the possible ligations and scissions which are possible for polymers of length up to a maximum $l_{\max}$, a particular reaction is included in a realization of the model. To generate general conclusions in the absence of detailed knowledge of the rates of such reactions in terrestrial or putative extraterrestrial biochemistry, we generate a large (typically 10^4) set of "artificial chemistries" consistent with the parameter p and then compute probabilities of various types of occurrences by averaging over the resulting ensemble of artificial chemistries and dynamic realizations. The algorithm for generating, given p, an artificial chemistry on a single chemically "well-mixed" site is the same as that fully described and used in Ref. [4]. In the work described here we use the same procedure to generate chemical networks and then distribute identical copies of each such network on all the sites of the spatial lattice in order to carry our dynamical simulations. The dynamics of the model described here differs from that in [4] because the transfer of molecules between the sites is an allowed dynamical event as described below and in Appendix A. Some discussion of the choice to use identical chemical networks on all the sites appears below.

As before, population dynamics are computed only for networks which are "viable," by which we mean that there is at least one reaction path from a "food set," here chosen to be a set of monomers and dimers, to a polymer string of the largest allowed size. (In Ref. [4] the largest allowed polymer comprised ten monomers for most of the reported results, but here computational limitations have forced a limitation to a largest polymer length of six in most reported results.)

The population dynamics themselves are generated stochastically many times for each artificial chemical network. The results of these dynamical simulations are not identical, even when dynamics are carried out on identical chemical networks, because the dynamics are stochastic and, therefore, not deterministic. From the entire ensemble of dynamical results we then generate statistics for the probability of occurrence of various types of resulting steady states, deemed by one definition or another to be lifelike. (For example, in Ref. [4] we typically generated about 50 dynamic realizations for each chemical network and carried out simulations on roughly 10^4 chemical networks for each value of p.)

Fixing p and requiring viability on each site does not fully define the two-dimensional model of sites on a two-dimensional lattice. Options for fully defining the model include (i) generating an artificial chemical network consistent with p and then reproducing it on all the sites; (ii) generating a chemical network and reproducing it on each site, but assigning different reaction rates v [as defined in Ref. [4] and in Eq. (1) below] to each chosen reaction in the network on different sites; (iii) generating different chemical networks, consistent with the same p, that are placed on each site (so that dynamics are carried out with different possible chemical reactions at each site); (iv) keeping only p the same on each site, so there are heterogeneous chemistries at each site, as in (iii), but lift the requirement that the networks on each island must be viable; or (v) placing different chemical networks at each site using a spatially dependent variation of p across the lattice of sites. Option (v) requires the introduction of new parameters to characterize any variation in p.

In the present paper, we report results on a model in which we took option (i). Because the dynamics are stochastically implemented, it will not necessarily be the case in option (i) that all of the sites will realize steady states in the same manner (if at all). An argument in favor of option (i) is that one might expect the laws of chemistry to be independent of the location of the reactants in space. On the other hand, chemical heterogeneity may be realized at different spatial sites due to spatial variation in such environmental variables as temperature or pH. Thus, options (ii) through (v) might roughly model real situations not realized by option (i). Many interesting new topological and dynamical possibilities arise in options (ii) through (v), and we plan to study them later.

Using option (i), we define a viable network as one which contains at least one reaction path allowing production of a polymer of maximum length starting from the food set. We only carried out dynamics simulations for those networks which were found to be viable, as in Ref. [4]. In the calculations giving the reported results, we used an 8×8 square lattice of sites with periodic boundary conditions and a maximum polymer size of six. The maximum polymer size is unfortunately small but was imposed by computational limitations. With an approximate periodicity determined by the parameter η, diffusive "hops" of randomly selected molecules were made from their resident site to one of its four neighbors. The precise relation of η to the number of diffusive events is described in Appendix A, where a review of the Gillespie algorithm [8] used in the dynamics simulations also is presented. Roughly, η is the fraction of dynamical events, which include both reactions and diffusive hops, which are diffusive hops. An interesting

and somewhat unexpected result to be discussed in more detail below is that the model only exhibits interesting behavior at low diffusion, i.e., at small values of η.

The chemical dynamics of the model has the same form within each site as that for the single-site model described in [4] and is governed by stochastic implementation of the probabilities described in the master equation,

$$dn_l/dt = \sum_{l',m,e} [v_{l,l',m,e}(-k_d n_l n'_l n_e + k_d^{-1} n_m n_e) + v_{m,l',l,e}(+k_d n_m n'_l n_e - k_d^{-1} n_l n_e)], \quad (1)$$

where n_l is the number of polymers of species l, $v_{l,l',m,e}$ is proportional to the rate of the reaction $l + l' \xrightarrow{e} m$, e denotes the catalyst, l and l' denote the polymer species combined during ligation or produced during cleavage, and m denotes the product of ligation or the reactant during cleavage. As discussed in Ref. [4], the parameter k_d is a rough proxy for the effects of temperature in the model. As before, in the simulation results reported here we set $k_d = 1$ corresponding to "infinite temperature," which simply means that forward and reverse reactions have equal probability.

In the dynamics portion of the code within this model, we added a procedure to check, during each dynamic simulation, that the calculated ratio of instantaneous to equilibrium entropy had reached steady state as described in Appendix B. This was done because, with very small η values, the dynamical simulations took significantly longer to reach steady state than they had in the single-site case, and we needed to both be sure that the systems were, in fact, in steady state and to save computational resources by not carrying out excessive computational simulation after steady state had been reached.

III. INSTANTANEOUS, PARTIALLY EQUILIBRATED, AND GLOBALLY EQUILIBRATED ENTROPIES

The number of spatial islands is set to a value M (here 64) and the maximum polymer length to a value $l_{\max}$ (here 6). A fine-grained, "microscopic" description of a state is given by a $(2^{l_{\max}+1} - 2)M$-tuple of integers $\{n_{l,i}\}$, where l labels specific species as in Ref. [4] and $n_{l,i}$ is the number of polymers of species l on site i. Generalizing the coarse-graining procedure used in Ref. [4] for a single site, we introduce a coarse graining that is specified by the set of numbers $\{N_{L,i}\}$, where $N_{L,i}$ is the number of polymers of length L on site i. There can be a further coarse graining to describe a "macrostate" within our multisite model by specifying solely the set of numbers $\{N_L\}$, where $N_L = \sum_{i=1}^{M} N_{L,i}$ is the total number of polymers with length L in the system. With this notation one finds the number W_{global} of microstates associated with the coarser macrostate specified by $\{N_L\}$ to be

$$W_{\text{global}}(\{N_L\}) = \prod_L \frac{(N_L + 2^L M - 1)!}{(2^L M - 1)! N_L!} = \prod_L \sum_{\sum_i N_{L,i} = N_L} \prod_{i=1}^{M} \frac{(N_{L,i} + 2^L - 1)!}{(2^L - 1)! N_{L,i}!}. \quad (2)$$

A formal derivation of the second equality appears in Appendix C. We refer to $S_{\text{global}} = \ln W_{\text{global}}$ as the instantaneous global entropy.

Maximizing $\ln(W_{\text{global}})$ subject to the condition $\sum_L N_L = N$ (the total number of polymers in a system) gives

$$S_{\text{global,eq}}(N) = (MG_{l_{\max}} - l_{\max}) F\left(\frac{N}{MG_{l_{\max}} - l_{\max}}\right) \quad (3)$$

for the equilibrium global entropy. Here $F(x) = (1 + x)\ln(1 + x) - x \ln x$, Stirling's approximation has been used, $G_{l_{\max}} = 2^{l_{\max}+1} - 2$, and the Boltzmann constant (k_B) has been dropped for convenience. This entropy maximization corresponds to fully equilibrated populations of $N_{L,i} = g_L N/(MG_{l_{\max}})$ for polymers of length L at site i, where $g_L = 2^L - 1$.

At the less coarse-grained level, corresponding to specifying the set of numbers $\{N_{L,i}\}$, we define a local entropy S_i at each site,

$$S_i(\{N_{L,i}\}) = \sum_L \ln\left[\frac{(N_{L,i} + 2^L - 1)!}{(2^L - 1)! N_{L,i}!}\right], \quad (4)$$

and a total local entropy,

$$S(\{N_{L,i}\}) = \sum_{i=1}^{M} S_i(\{N_{L,i}\}). \quad (5)$$

From the second expression for W_{global} above (as derived in Appendix C) we then have

$$S_{\text{global}}(\{N_L\}) = \ln\left\{\sum_{\sum_i N_{L,i} = N_L} \exp[S(\{N_{L,i}\})]\right\}. \quad (6)$$

From this it is easy to show that it will always be the case that $S_{\text{global}} \geqslant S$ with the equality only holding approximately if the sum in the exponent on the right of the expression above relating S_{global} to S is dominated by its largest term. These nonequilibrium quantities can both be evaluated using the instantaneous values of $\{N_{L,i}\}$ at any time during the simulation. We show some examples of such evaluations in Fig. 2. As expected, the inequality is always obeyed, but the conditions for the near equality are not always met.

If we maximize S subject only to the constraint $\sum_{L,i} N_{L,i} = N$, then we find

$$S_{\text{eq}}(N) = MG_{l_{\max}} F\left(\frac{N}{MG_{l_{\max}}}\right), \quad (7)$$

which is close to but less than the maximum value of S_{global} given by Eq. (3). In our simulations $MG_{l_{\max}} - l_{\max} = 64(2^7 - 2) - 6 = 16\,250$, whereas $MG_{l_{\max}} = 16\,256$ so the difference is negligible and will shrink further for larger $l_{\max}$. Thus, we see that, at equilibrium, the sum in (6) is very nearly dominated by its largest term and maximizing either S or S_{global} leads to global equilibrium with the population distributions $N_{L,i} = g_L N/(MG_{l_{\max}})$.

We now consider the possibility of partial equilibrations, focusing attention on S. We can maximize S as a function of the set of numbers $\{N_{L,i}\}$ for fixed values of $\{N_L\}$ without requiring that the values $N_{L,i}$ within a site take the equilibrium values resulting from the reactions within each site. We refer

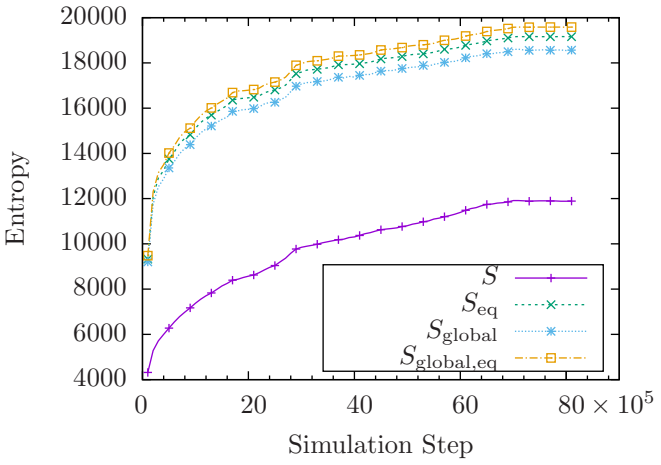

FIG. 2. Instantaneous, global, and globally equilibrated entropies as a function of the number of reaction steps for a realization of the dynamics with $p = 0.00761$ and $\eta = 10^{-7}$.

to this as "diffusive equilibration," and we expect it to occur for sufficiently large values of η. Maximizing S subject to the conditions $\sum_i N_{L,i} = N_L$ gives

$$S_{\text{diff eq}}(\{N_L\}) = M \sum_L g_L F\left(\frac{N_L}{g_L M}\right), \tag{8}$$

in which $F(x) = (1+x)\ln(1+x) - x\ln x$ as before (but x has a different value). In this case, the equilibrium values for the number of polymers of length L at site i is given by $N_{L,i} = N_L/M$, which intuitively is expected in diffusive equilibrium. If the instantaneous state is close to this diffusively equilibrated state with $N_{L,i} = N_L/M$ but far from the fully equilibrated state with $N_{L,i} = g_L N/(M G_{l_{\max}})$, then we refer to the system as DDLA.

Turning to the other type of partial equilibration, we maximize S subject to the conditions that the numbers of polymers at the sites, i.e., $N_i = \sum_L N_{L,i}$, are fixed, but we do not require that $N_L = \sum_i N_{L,i}$ be fixed. In this way, the maximization takes account of equilibration through the chemical reactions within each site but does not require diffusive equilibrium. The resulting partially equilibrated entropy is found to be

$$S_{\text{chem eq}}(\{N_i\}) = G_{l_{\max}} \sum_i F(N_i/G_{l_{\max}}) \tag{9}$$

and the corresponding population distribution is $N_{L,i} = g_L N_i/G_{l_{\max}}$. When the instantaneously evaluated values of $N_{L,i}$ are close to this distribution but far from the fully equilibrated distribution $N_{L,i} = g_L N/(M G_{l_{\max}})$, then we refer to the system as DALD.

If the instantaneous values $N_{L,i}$ are far from both partially equilibrated distributions we refer to the system as DALA. The quantitative definitions chosen to characterize "close to" and "far from" in these descriptions are provided in the next section.

IV. DISCRIMINATING PARTIALLY EQUILIBRATED FROM FULLY NONEQUILIBRIUM STATES IN THE SIMULATIONS

Though the partially equilibrated states defined above are well defined, it is not sufficient to compare the instantaneous value of S to the partially equilibrated values in order to determine whether the instantaneous state is partially equilibrated in one of the states defined. Instead, we consider the position of the state in the space of "macrostates" defined by the set of variables $\{N_{L,i}\}$. The number of these variables is $l_{\max}M$, which in our simulations is 384 and is to be contrasted with the "microstate" specification in terms of the variables $\{n_{l,i}\}$, of which there are $MG_{l_{\max}}$, which is 8064 in our simulations.

We have shown above that when S is maximized at fixed $N_L = \sum_i N_{L,i}$, which we call diffusive equilibration, then the set of numbers $\{N_{L,i}\}$ take the values $N_{L,i} = N_L/M$. We can regard this maximization as taking place in a hyperplane in the space of macrostates defined by the constraint equations, of which there are $l_{\max}$, so the hyperplane has dimension $(M-1)l_{\max}$. We denote the partially equilibrated position $N_{L,i} = N_L/M$ in that hyperplane by P_d (which is a 384-tuple of numbers). Similarly, we showed that if we maximize S at fixed $N_i = \sum_L N_{L,i}$, then the maximum occurs at the point $N_{L,i} = g_L N_i/G_{l_{\max}}$. That maximization takes place in another hyperplane of dimension $M(l_{\max}-1)$. We denote that point of chemical equilibration by P_c. We provide a simplified sketch to illustrate the situation in Fig. 3.

In the simulations reported below, there is another constraint, namely that the "food" populations on each site are

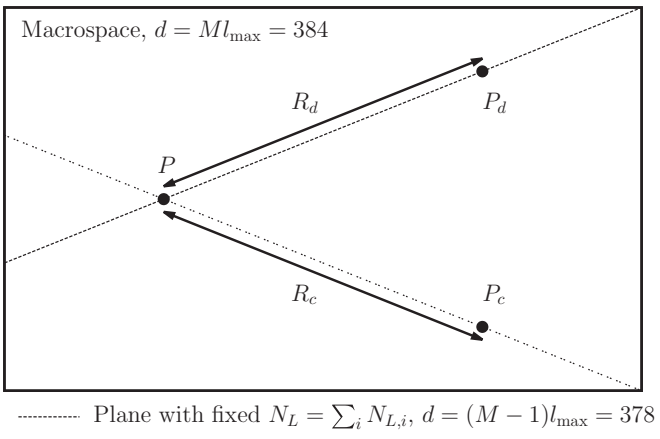

FIG. 3. Illustration of the geometry of the macrospace in which partial equilibrations can take place. P represents the $Ml_{\max}$-tuple $\{N_{L,i}\}$ of instantaneous populations during the simulation. P_d is the $Ml_{\max}$-tuple of populations which maximize the entropy S under the constraint $N_L = \sum_i N_{L,i}$ and P_c is the $Ml_{\max}$-tuple of populations which maximize the entropy S under the constraint $N_i = \sum_L N_{L,i}$. The plane illustrated is the two-dimensional plane in which the two $Ml_{\max}$-dimensional vectors P_c-P and P_d-P lie. The lines between them in the picture are the projections of the hyperplanes defined by the constraints $N_i = \sum_L N_{L,i}$ and $N_L = \sum_i N_{L,i}$ onto the plane of the figure. The quantities R_c and R_d are the Euclidean norms of those vectors as defined in Eqs. (10).

kept at a fixed value (50 in the reported results) and are therefore not expected to equilibrate. Thus, the relaxation toward equilibrium to which the discussion in this section applies is actually carried out numerically in the chemical space not including the food set, and so the dimensions in Fig. 3 are all reduced by 128 (=$2M$, since the food set consists of polymers of length one and two).

At any point during the simulation we have values of the variables $\{N_{L,i}\}$ and easily compute the coordinates of the instantaneous point P in the macrospace (which is just given by the values of $\{N_{L,i}\}$) and of the partially equilibrated points P_d and P_c from those values. To determine how close the instantaneous values of the macrovariables are to partial diffusive or partial chemical equilibration, we compute the Euclidean distances in the macrospace between the instantaneous point P and the partially equilibrated points P_d and P_c, denoting the distances by R_d and R_c, respectively:

$$R_c = \sqrt{\sum_{L,i}(N_{L,i} - g_L N_i / G_{l_{\max}})^2},$$
$$R_d = \sqrt{\sum_{L,i}(N_{L,i} - N_L/M)^2}. \tag{10}$$

If a system is fully globally equilibrated, both values will be near zero, but cases in which one value is small and the other is large are realized in the simulations and provide a quantitative definition of the meaning of partial equilibration in the two senses discussed. We are only interested in states for which the instantaneous calculated entropy S [found from Eq. (5)] is less than its fully equilibrated value [found from Eq. (7)], following our earlier postulate that lifelike states must not be in full equilibrium [4]. Given that constraint, we then separate the entropically steady states which we find to be out of equilibrium by values of R_c and R_d. We find, as we show below, that they fall roughly into classes characterizable as DDLA (small R_d, large R_c), DALD (large R_d, small R_c), and DALA (large R_d and R_c). An appropriate normalization for the values of R is $1/(\sqrt{2}N)$, where N is the total number of polymers, because it is easy to show that the maximum value of R at given N is $\sqrt{2}N$.

V. RESULTS FOR FREQUENCY DISTRIBUTIONS OF UNEQUILIBRATED AND PARTIALLY EQUILIBRATED STATES

In Figs. 4 and 5 we show three-dimensional scatter plots indicating the steady-state values of the quantities $R_d/(\sqrt{2}N)$ and $R_c/(\sqrt{2}N)$ for systems in entropically steady states such that $S/S_{\text{global,eq}}$ is less than 0.6 and thus out of global equilibrium. As noted at the end of the last section, these results are obtained by use of the population statistics of the "nonfood" populations only, excluding the six species of "food" polymers of lengths one and two whose total populations per site are held at 50. Scatter plots are shown for several values of the parameters p and η.

In these and other results reported in this paper we have not applied the dynamical constraint discussed in [4] when selecting states deemed lifelike. That constraint assured that the states selected continued to behave in a sufficiently dynamical manner though the ratio of the entropy to its equilibrium value had reached steady state. The dynamical constraint was not used here because doing so imposed an unacceptable numerical burden in this larger system. However, we have made calculations in a few cases, as reported in Sec. VII, which suggest that adding the dynamical constraint does not change the overall dependence of lifelike frequencies on p and η significantly, though the number of states deemed lifelike is reduced.

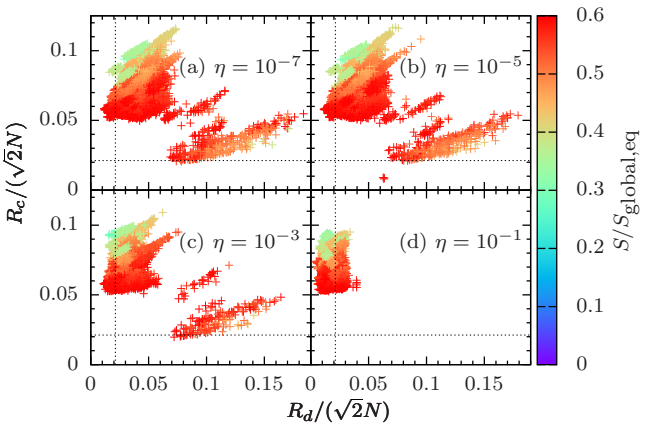

FIG. 4. Scatter plots of the normalized distances from partial equilibria on the horizontal and vertical axes and their entropy ratio denoted by the point color for $p = 0.00320$ and differing values of η. Of 10^5 randomly constructed networks, the ones deemed viable had 50 ensembles simulated each with a different initial condition and plotted. The dashed lines denote the cutoff values of $0.03/\sqrt{2}$ used for the different classifications of lifelike.

As discussed, the entropically steady state values fall roughly into three groups: those with small $R_d/(\sqrt{2}N)$ and large $R_c/(\sqrt{2}N)$, which are regarded as DDLA; those with small $R_c/(\sqrt{2}N)$ and large $R_d/(\sqrt{2}N)$, regarded as

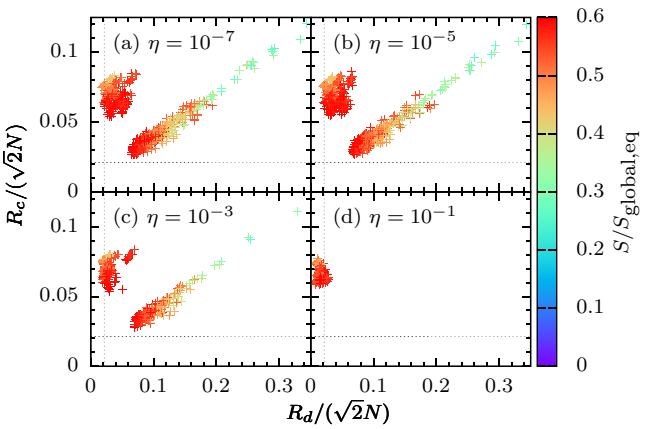

FIG. 5. Scatter plots of the normalized distances from partial equilibria on the horizontal and vertical axes and their entropy ratio denoted by the point color for $p = 0.00761$ and differing values of η. Of 10^4 randomly constructed networks the ones deemed viable had 10 ensembles simulated, each with a different initial condition and plotted. The dashed lines denote the cutoff values of $0.03/\sqrt{2}$ used for the different classifications of lifelike.

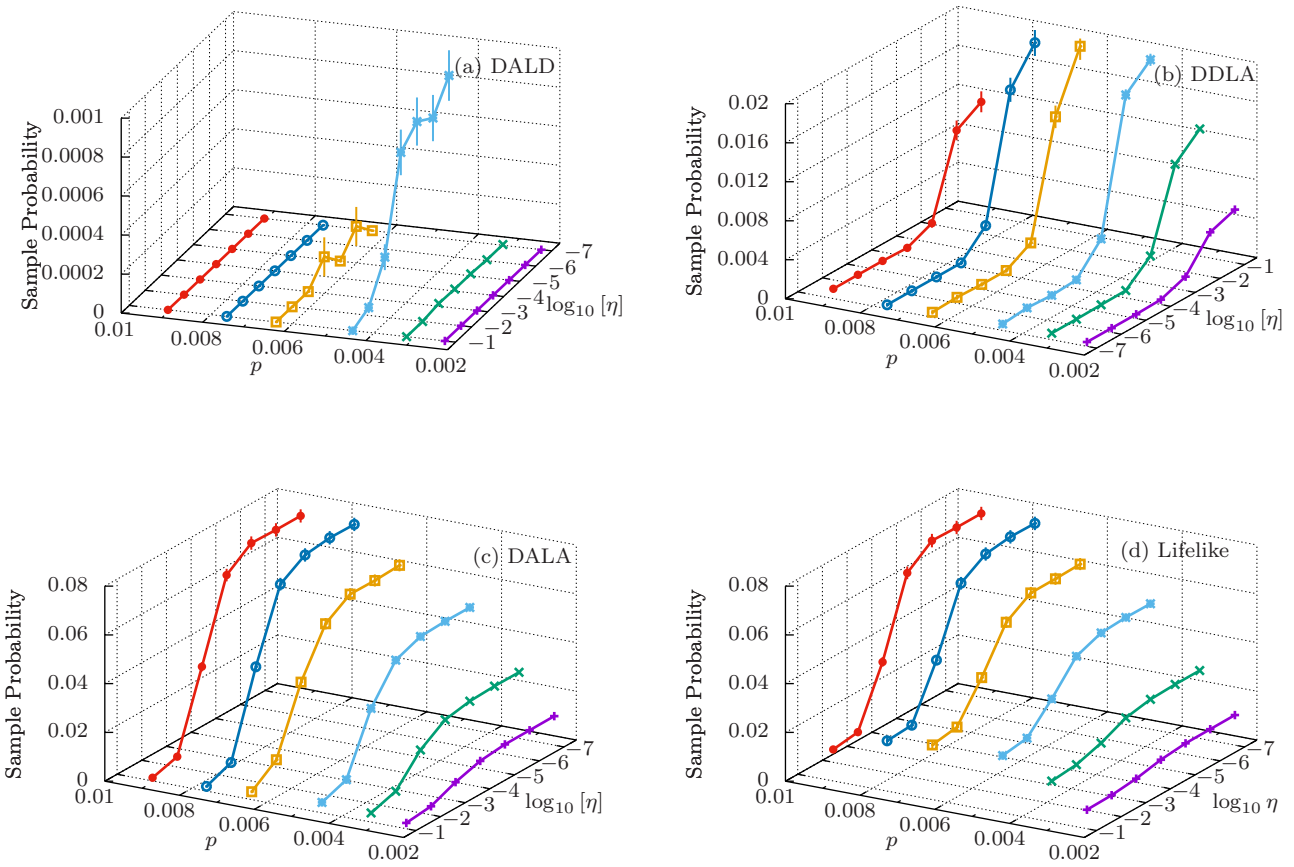

FIG. 6. The probabilities of forming the different lifelike states DALD (a), DDLA (b), and DALA (c), as well as the probability of the system being generally lifelike ($S/S_{\text{global,eq}} < 0.6$) in (d) given a random network formed with parameter p and simulated with hopping parameter η. [The sum of the values in (a), (b), and (c) yields (d).]

DALD; and those with both $R_c/(\sqrt{2}N)$ and $R_d/(\sqrt{2}N)$ large, regarded as DALA. By choosing, somewhat arbitrarily, cutoffs of $0.03/\sqrt{2}$ on $R_c/(\sqrt{2}N)$ and $R_d/(\sqrt{2}N)$ to define these different types, we can get an overview of the parameter dependence of the likelihood of these different types of steady states as indicated in Fig. 6.

The sample of results shown in Figs. 4 and 5 are quite characteristic in showing that DALD states, which would occur near zero along the horizontal axes of the figures are quite rare [data on their abundance appears in Fig. 6(a)]. DDLA states [with probability distributions shown in Fig. 6(b)] appear along the vertical axes and match the behavior we observed in the single-site studies of Ref. [4] at large η quite well, as shown in Fig. 7. These states are essentially spatially homogeneous copies of our previous single-site results.

The most unexpected results are the DALA states appearing as a band along a diagonal line in the R_c-R_d plane, which is particularly evident in Fig. 5, though similar, sometimes more complex, distributions appear in that region for other values of p as seen in Fig. 4.

The distribution of DALA states as a function of p and η appears in Fig. 6(c). Of particular interest with regard to the DALA distribution is the fact that the DALA states appear for quite large values p, where our single-site model gave mainly chemically equilibrated systems. In terms of our postulated criterion for "lifelike" states, namely that they should be out of equilibrium, these states seem to be attractive candidates for a new kind of lifelike state in the model. Accordingly, we explored their nature further, as described in the next section.

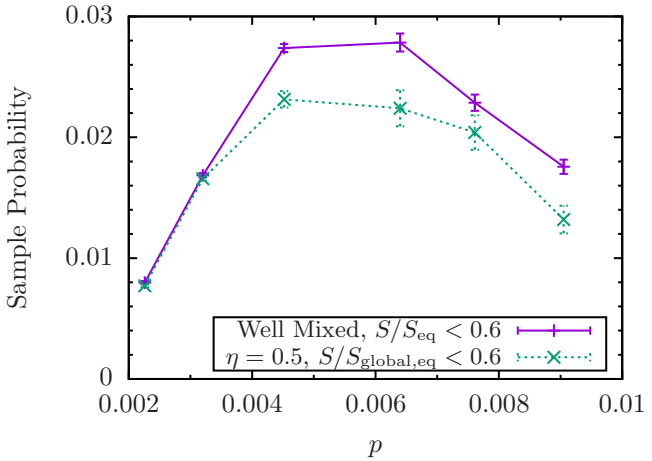

FIG. 7. Comparison of results for the probability of occurrence of steady states with $S/S_{\text{eq}} < 0.6$ in the single-site, well-mixed, model of Ref. [4] (with $l_{\max} = 6$) with results for the probability of occurrence of states with $S/S_{\text{global,eq}} < 0.6$ in the model of this paper with $\eta = 0.5$ and $l_{\max} = 6$.

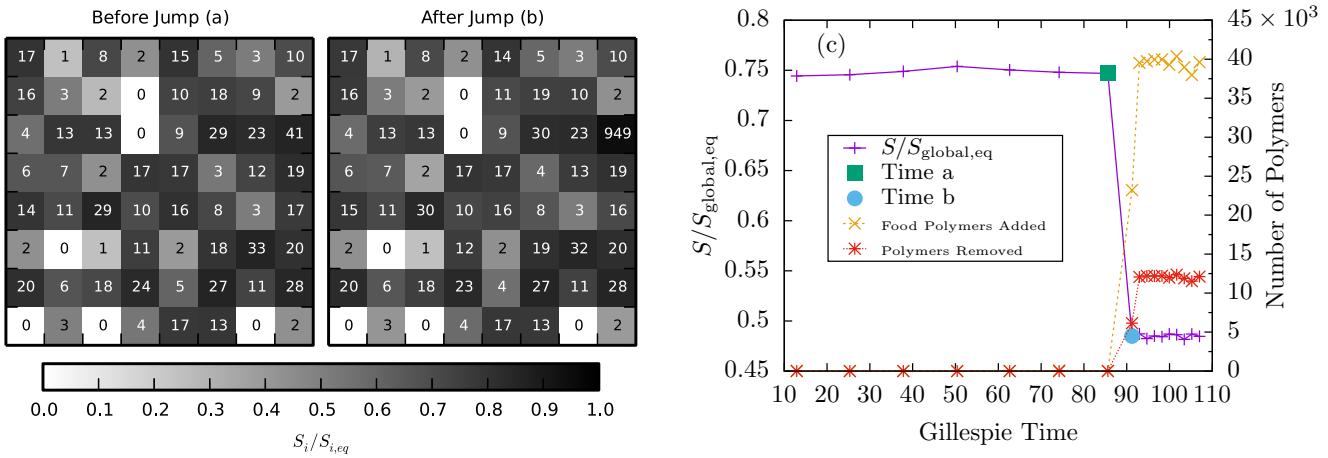

FIG. 8. Example of a DALA dynamics run in which a site explosion occurred for $p = 0.006\,40$ and $\eta = 10^{-7}$. Panels (a) and (b) show the state of the system before and after the single-site population explosion. The grid represents the lattice. The shade of the square is the single-site entropy ratio as defined in Ref. [4], with the scale located below the plots, and the number written is the total population of nonfood particles. (There are at least 50 food particles on each site.) Panel (c) is the entropy ratio on the left y axis as well as the food polymers added and polymers removed on the right y axis as a function of time with the entropy ratios before and after the population explosion marked.

VI. DALA AND DALD STATE ANALYSES AND POPULATION GROWTH RATES

An interesting and surprising result is that many DALA states occur at small values of η, as expected, but at relatively large values of p at which our earlier one-site studies would suggest that local (chemical) equilibrium would commonly occur. To study these states further, we have explored their detailed dynamical history in some cases, as illustrated in Fig. 8. In these cases, after an initial, apparently stable, steady state exhibiting similar (though not identical) out-of-equilibrium behavior on all sites, a single site suddenly and explosively grows in population to completely dominate the total population, after which the system subsides into a new metastable state with a lower entropy ratio $S/S_{\text{global,eq}}$. The site with dominant population (typically nearly 50 times larger than other sites) has a single-site entropy which is nearly in chemical equilibrium, while the other sites remain far from chemical equilibrium. At the "exploded" site an analysis of the flows, illustrated in Fig. 8, shows that the site has saturated the limit of 950 nonfood polymers per site and polymers are being removed as well as added to maintain the food set at the minimum value taken to be 50 here. It appears, however, that the "explosion" may be triggered by a rare diffusive transfer of a molecule from a neighboring site as discussed below.

These explosive events can occur more than once in a simulation run, as shown in Fig. 9, leading to an additional high-population site at each explosive growth episode. Sometimes the high-population states occur together in space but in other cases they are widely separated. We computed the correlation function of the populations on different sites over the ensemble of DALA, as shown in Fig. 10. Figure 10 shows that, on average, there are correlations between the populations on different sites which grow stronger as η increases, as expected intuitively.

In order to distinguish the states with explosive sites from those without explosive sites, we define a steady state to have a disproportionate population spread (DPS) if there is at least one site with a nonfood population of over 900 and at least one site with a nonfood population of less than 100. Using this classification of states represented by points in the DALA region of the scatter plots in Figs. 4 and 5 gives results shown in Fig. 11. Comparing Figs. 5(b) and 11(c) and 11(d) indicates that, at least when $p = 0.00761$ and $\eta = 10^{-5}$, the diagonal band of DALA states are essentially all of the exploding, DPS, type. This pattern is repeated for most of the studied values of p though, as illustrated by comparing Fig. 4(b) with Figs. 11(a) and 11(b) for $p = 0.00320$ and $\eta = 10^{-5}$, the situation is more complex in some cases (The range of p's explored is shown in Fig. 6).

Computing the frequencies with which the states previously classified as DALA were also of the exploding, DPS, type occur in the ensemble of dynamically simulated states yields Fig. 12. Comparing Fig. 12 with Fig. 6(c) indicates that most (roughly 70%) of the states classified as DALA are of the exploding, DPS type. The other states classified as DALA are similar to the DDLA states. At large η they appear to be similar to the nonequilibrium states found in [4].

We further investigate the DALA DPS and non-DPS states by studying the nonfood polymer population growth rate. In Fig. 13 we plot the values of the logarithmic derivative of $S/S_{\text{global,eq}}$ with respect to the real (Gillespie) time on the vertical axis and the corresponding logarithmic derivative of the nonfood molecule population on the horizontal axis. Each point gives the average value of these two quantities for a different dynamical system while it is in an entropic steady state as determined by our code. Results are shown for DPS and non-DPS DALA states and $\eta = 10^{-5}$ with $p = 0.00761$ in Fig. 13. As expected, the points cluster around zero on the y (entropy growth rate) axis as the code selects states in entropic steady state, as explained in Appendix B. For most values of p and η results like those in Figs. 13(a) and 13(b) for $p = 0.00761$ are seen so that, unlike our previous results on single sites, the population of many of the DPS states with exploding

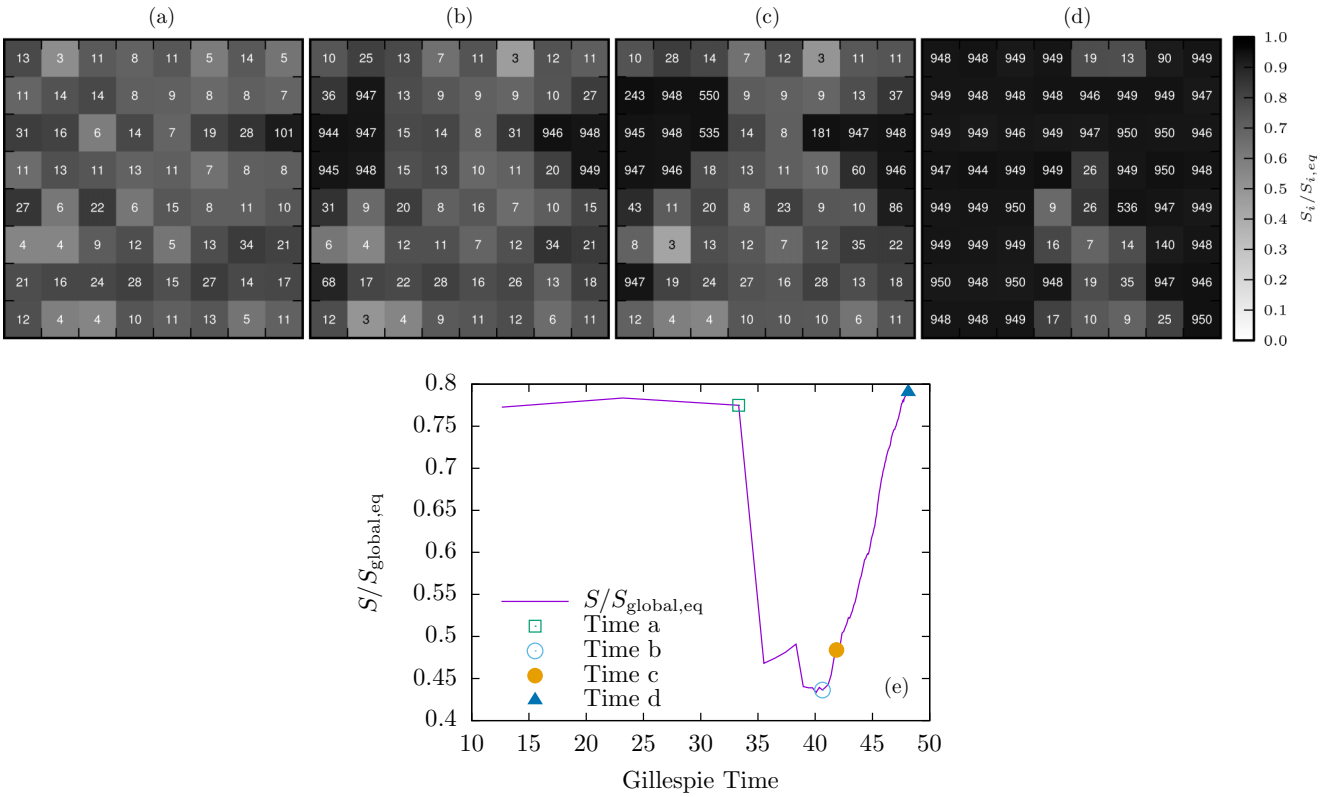

FIG. 9. An example of a dynamics run in which multiple site explosions occurred with $p = 0.006\,40$ and $\eta = 10^{-2}$. Panels (a), (b), (c), and (d) depict the system at different points in time with entropy ratios shown in (e). In (b), a cluster of exploded sites appears which was apparently produced when polymers diffused from the initial exploded site to its neighbors causing them to explode. In panel (c) a site near the lower left corner has exploded independently of the larger cluster. The entropy ratio first drops with successive explosions and then rises to the full equilibrium value as the region of exploded sites expands to fill the entire lattice.

sites is exponentially growing in time. Though exponential population growth may suggest possibilities of evolutionary phenomena within the model, it is not clear that these explosive DPS states should be regarded as lifelike, as discussed in the next section. We have not established that all of the states with exponentially growing populations have exploding sites. However, when we perform ensemble averages on the states represented by points in Fig. 13, we find that, on average, the DPS populations are growing exponentially in time and the non-DPS populations are not.

Combining these results, it is inferred that the DALA which do not have exploding sites (non-DPS states) are similar to those seen in Ref. [4], where we found a chemically nonequilibrated entropic steady state and very little population growth. Many DALA states have sites where the population has exploded and have reached local chemical equilibrium, while many sites in those states have low populations and nonequilibrium entropies. The very small values of $S/S_{\mathrm{global,eq}}$ in those states arise because the lattice is diffusively very far from equilibrium.

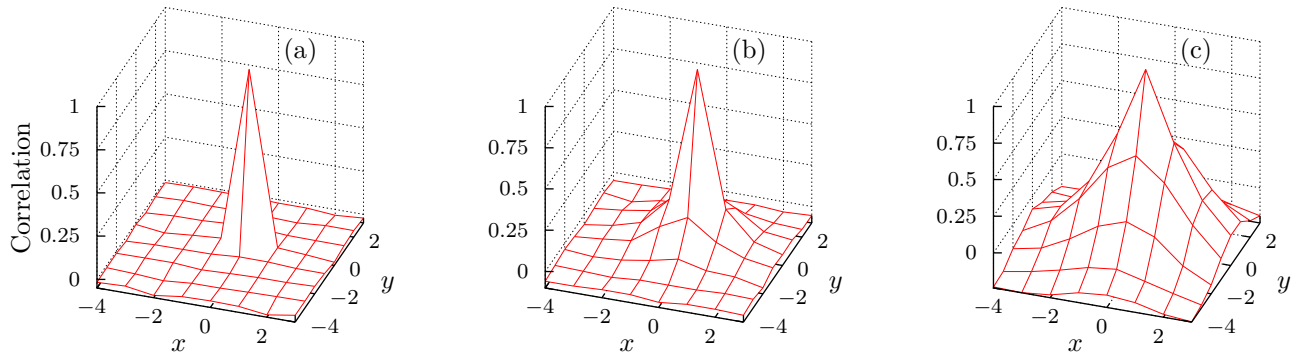

FIG. 10. The nonfood population correlation function as a function of site separation for DALA states with $p = 0.006\,40$ and varying values of η. The correlation function for which results are shown is $C(\vec{r}) = \tilde{C}(\vec{r})/\tilde{C}(0)$, where $\tilde{C}(r) = (1/M)\sum_{\vec{r}'} N_{\mathrm{nf}}(\vec{r}')N_{\mathrm{nf}}(\vec{r}' + \vec{r}) - (1/M)\sum_{\vec{r}'} N_{\mathrm{nf}}(\vec{r}')^2$ and $N_{\mathrm{nf}}(\vec{r})$ is the number of nonfood polymers at site $\vec{r}$. η values are (a) $\eta = 10^{-4}$, (b) $\eta = 10^{-3}$, and (c) $\eta = 10^{-2}$.

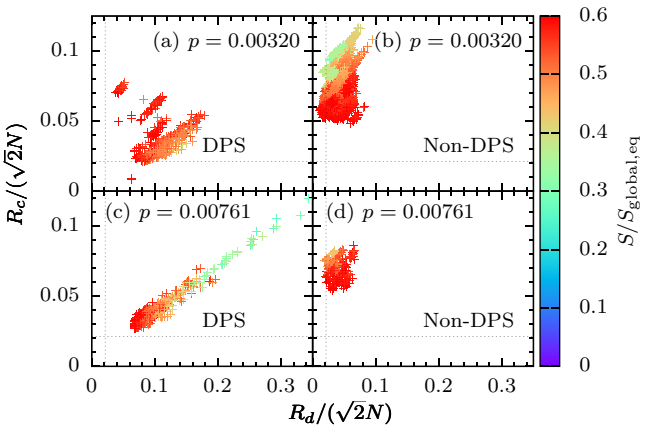

FIG. 11. The same as Figs. 4(b) and 5(b) and $\eta = 10^{-5}$, except partitioned based on whether the system is of the exploding "DPS" type.

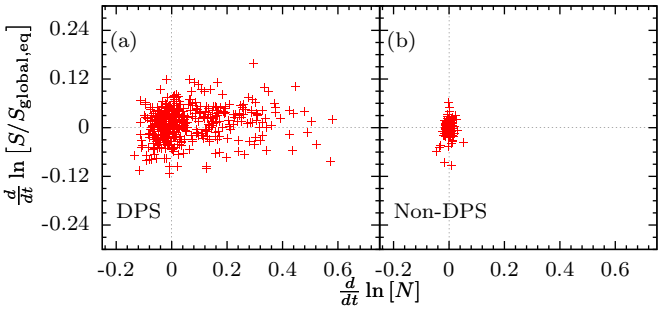

FIG. 13. The logarithmic derivative of the nonfood polymer population and the entropy ratio of the explosive and nonexplosive systems for DALA states for $p = 0.00761$ and $\eta = 10^{-5}$. In general, the growth of the explosive systems had some nonzero polymer population growth while the nonexplosive systems growth centered around zero. A similar, but less clear, distinction was observed for other p values.

Individual sites in the DALD states are closer to chemical equilibrium than those in the DALA states, as expected. Detailed inspection of the temporal history of several DALD states reveals sites with exploding populations as in the DALA states. The exploding sites in DALD states appear much faster and grow at a slower rate than those in the DALA states, so that the temporal transition to a low-entropy state is less sharp, as illustrated in Fig. 14.

VII. DISCUSSION AND CONCLUSIONS

Extending our previous model by reproducing it on the sites of a lattice and allowing diffusion of molecules between the sites, we have numerically explored the probability and nature of dynamical nonequilibrium states as a function of the parameters p and η which, respectively, control the chemical reaction and diffusion rates. For large η we see results which are similar to those obtained earlier [4] for single sites. For smaller η we distinguish nonequilibrium states which are partially equilibrated with respect to chemical reactions but not diffusion (DALD), with respect to diffusion but not chemical reactions (DDLA), and with respect to those that are not partially equilibrated in either sense (DALA). The frequencies with which these different nonequilibrium states appear in our numerical model of 8×8 sites on a square lattice as a function of p and η is summarized in Fig. 6. DALD states appear rarely in a restricted range of p at small η. DDLA states appear at larger η in a fashion whose p dependence mirrors that found earlier for single sites. These states appear to consist essentially of reproductions of our previous results on all the sites.

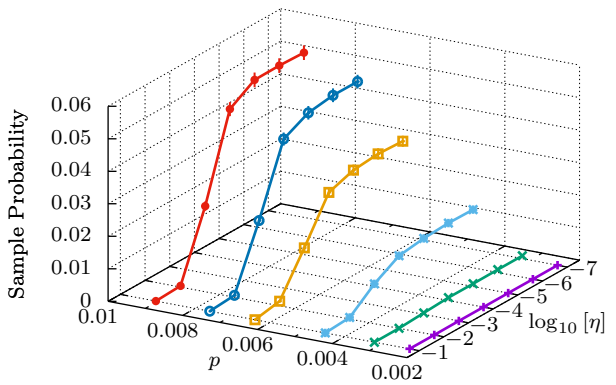

FIG. 12. Probabilities of DALA states with a disproportionate population spread (DPS).

The distribution and nature of the DALA states was unexpectedly interesting. They occur with relatively high frequency at p values, which are large enough to drive most single sites to equilibrium, and at small η. Exploring the nature of the DALA states in more detail, we found that they fall broadly in two groups, as illustrated in the scatter plots in Fig. 5. The less interesting group is qualitatively similar to the DDLA states, and those states were classified as DALA only as a consequence of our choice of cutoff for nonequilibrium states in the definition of DALA. The more interesting group is represented by the states scattered along a diagonal in Fig. 5. As discussed and illustrated in Figs. 6 and 8, they consist almost entirely of systems in which a small fraction of the 64 sites have, suddenly on the Gillespie real-time scale, "exploded" in the sense that their population has begun to grow exponentially in time while their local entropy goes to equilibrium.

We find that the source of the material feeding these explosions comes from the local food source, which is maintained at a fixed value in the simulation. It does not necessarily arise from diffusion of particles from the surrounding sites, which remain locally out of equilibrium and lifelike by our previous single-site criterion. There is some evidence, not yet fully confirmed, that the explosions are triggered by the diffusion of one or a few particles into the site which explodes. The triggering seems to usually occur more than 10^5 reaction steps before the explosion is fully developed. Running these simulations further we usually find a series of population explosions, separated by periods of steady-state entropy. Each explosion causes a precipitous drop in the ratio of the total local entropy to its fully equilibrated value associated with the highly spatially heterogeneous nature of the resulting state. Often, but not always, the explosions occur at sites neighboring previously exploded sites, so that a cluster of exploded sites

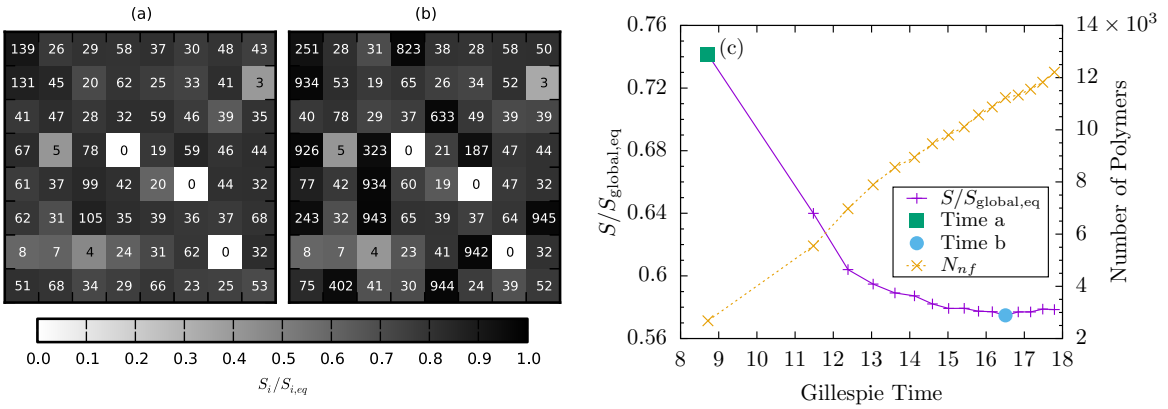

FIG. 14. An example of a DALD dynamics run with $p = 0.00452$ and $\eta = 10^{-6}$. Panels (a) and (b) show the state of the system at specific times in the run and (c) is the entropy ratio and the total number of nonfood polymers (N_{nf}) as a function of time.

develops. When the number of exploded sites becomes very large, the entropy rises again as the system becomes fully equilibrated both diffusively and chemically, as illustrated in Fig. 9.

To develop a statistical measure of the likelihood of these exploding sites, we quantitatively characterized a state with disproportionate population spread (DPS) which distinguishes these states from DALA states which are similar to DDLA states (that is spatially nearly homogeneous but out of chemical equilibrium), with results shown in Fig. 11. The DPS states occur at small η and large p with the indicated frequencies. They are exponentially growing in population while the ratio

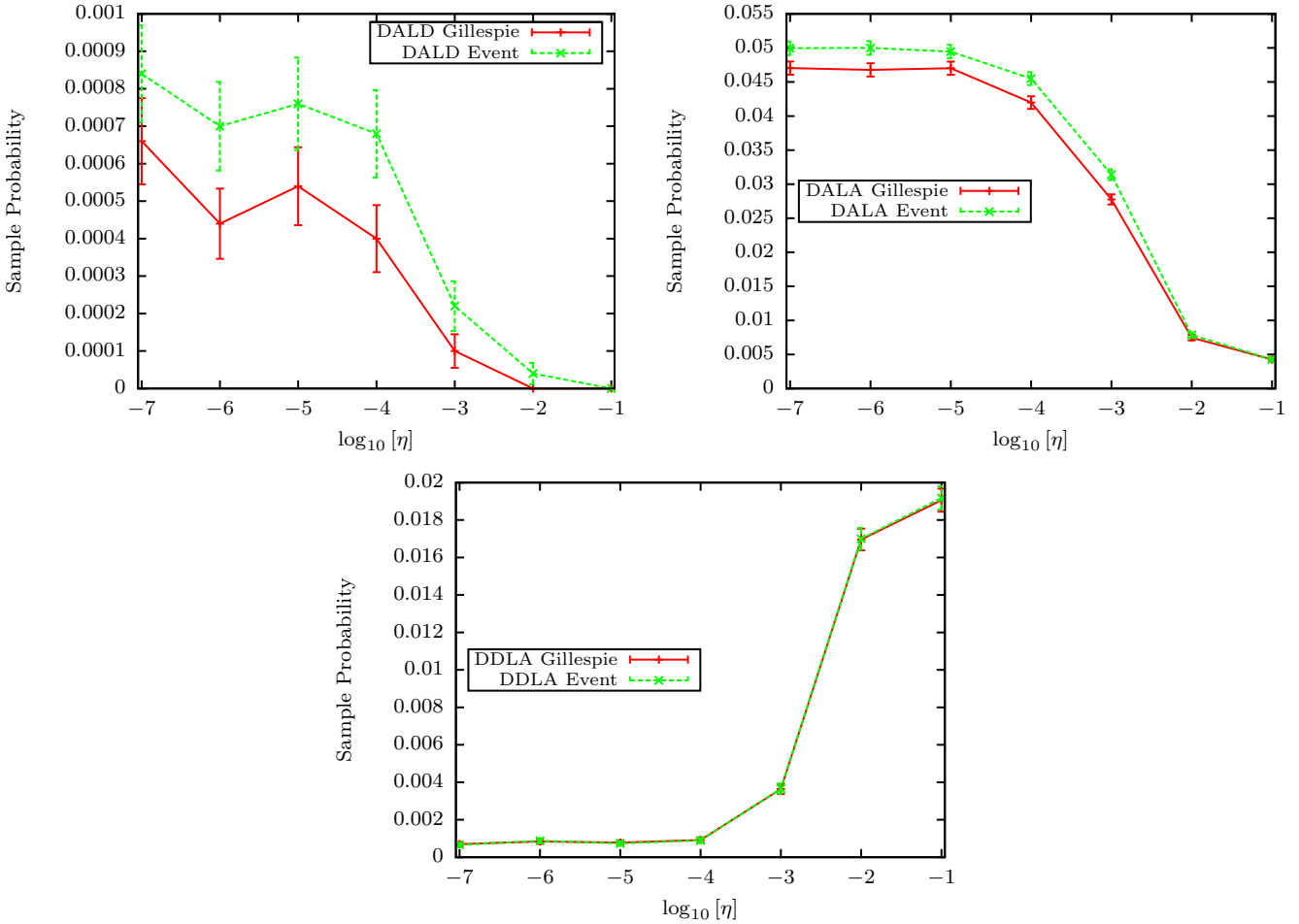

FIG. 15. Effects on the probability of occurrence of DALD, DALA, and DDLA states on the use of the "real" Gillespie time to determine that the system is in steady state; $p = 0.00452$.

of their global entropy to its equilibrium value remains nearly constant as illustrated in Fig. 13.

It remains to determine what, if any, significance these results may have for evaluating the probability that a set of interacting spatially separated but diffusively coupled chemical systems might evolve prebiotically to a recognizable precursor of a biological system. Our previous single site criterion for classifying a system as lifelike was that a lifelike system should be dynamic and out of chemical equilibrium. If we extend that definition of lifelike to only require, in the spatially heterogeneous case, that the system be out of global equilibrium, then the DPS states which we have found certainly qualify as lifelike. On the other hand, looking in detail at the DPS states, one sees that such a conclusion is intuitively somewhat troubling: The exploding sites in DPS systems are locally near chemical equilibrium while their surroundings are out of equilibrium. There are some hints of cooperativity in the sense that diffusion events may trigger explosions, but cooperativity does not appear to be very extensive. Qualitatively, the dynamics of these DPS systems is somewhat reminiscent of what is seen in growth of biofilms [9] and in cancer [10], but it is unclear whether such similarities are significant or not. The DPS states appear to be at a kind of tipping point in which a small perturbation of the local nonequilibrium state at each site can trigger a sudden transition to a rapidly growing state with nearly equilibrium entropy. Models of some diseases, such as Alzheimer's disease [11], with a qualitatively similar structure have been reported.

We will, in the future, further explore the nature of these DPS systems, as well as the rare, but possibly more biologically significant, DALD systems, focusing particular attention on intersite correlations [4].

A technical issue which could alter features of the statistical distributions reported here is the definition of "steady state" we have used to select lifelike systems: We have numerically assumed here that a system is in steady state if its entropy has not changed significantly for 10^5 reaction steps, as explained in Appendix B. It can be argued that it would be more natural to define steady state in terms of the Gillespie real time. In the presence of exploding sites, the two measures of time will differ significantly. The lifetime of the steady states associated with DALA and DALD explosions is shorter in real time, because large populations shorten real Gillespie time relative to reaction step time. We show some results in Fig. 15, which indicate that the use of Gillespie time does reduce the probability of DALD and DALA states. The effect for this example is a reduction of not more than about 20% in the probability, and the shape of the curves describing the dependence on η is very similar to the one obtained using "event time" to determine the existence of steady state as described in Appendix B.

We made a few calculations in which we added dynamical constraint like the one used in Ref. [4] to the criteria for selection of entropically steady states as lifelike. We show a result in Fig. 16, which suggests that the main effect of such dynamical constraints will be to reduce the overall magnitude of the frequencies of occurrence of lifelike states without otherwise significantly changing the parameter dependencies of those frequencies. However, this point merits further investigation because we have preliminary indications that the dynamical nature of the entropically steady states changes significantly with η.

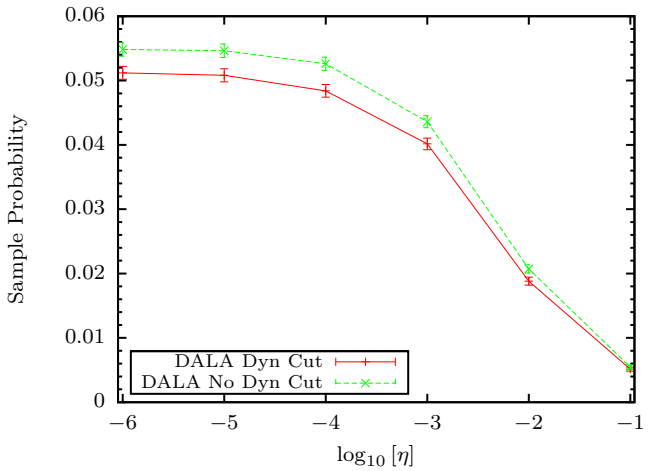

FIG. 16. The probability of forming a DALA lifelike state with $p = 0.00452$ and varying values of η with and without the dynamical constraint cut used in [4]. For the dynamical cut we require that $\omega_m > \omega_c$, where ω_m was determined from the (discretized) relation $\frac{\int_{-\omega_m}^{\omega_m} |C(\omega)d\omega|^2}{\int_{-\infty}^{\infty} |C(\omega)d\omega|^2} = 1/2$. Here $\omega_c = 0.0002(2\pi/\Delta t_{\rm ave})$, is a parameter of the model and $\Delta t_{\rm ave}$ is the average Gillespie time step. $C(\omega)$ is the time Fourier transform of $C(\tau) = (1/N_{\rm st}) \sum_{t,l,i} n_{l,i}(t) n_{l,i}(t+\tau)$, where $n_{l,i}(t)$ is the number of polymer species l on site i at time t. $N_{\rm st}$ is the number of discrete time steps in the sum on t.

Other issues that warrant additional exploration include the dependence of the observed phenomena on the availability of food. In the present calculations, food at each site was maintained externally at a fixed supply, and this provision is one reason that the DPS sites could grow without limit. For example, we will explore a model in which the total food supply in the entire system (but not at every site) is held fixed. This will mean that the exploding sites must depend on their neighbors to sustain their growth, which we would expect to have a significant influence on these systems.

ACKNOWLEDGMENTS

This work was supported by the United States National Aeronautics and Space Administration (NASA) through Grant NNX14AQ05G and used the computational resources of the Minnesota Supercomputing Institute, the Open Science Grid, the University of Minnesota School of Physics and Astronomy Condor cluster, and the NASA Advanced Supercomputing division Pleiades supercomputer. We also thank Simon Schneider for discussions.

APPENDIX A: DYNAMICS ALGORITHM

For network generation, the procedure described in Appendix A of [4] is used and the same network of reactions is copied onto each site of the spatial lattice. The dynamics algorithm is similar to that described in Appendix B of the same reference, but is altered to take account of spatial structure and diffusion. We assume that the rate of diffusive hops per

polymer is the same for all polymers and in all directions and is parametrized by the variable η, as described in more detail below. The dynamics routine makes use of the Gillespie algorithm [8], which permits efficient stochastic simulation of the master equation (1) for the chemical dynamics on each site, as was done in Ref. [4]. At the most microscopic level, states in the system at each time step are characterized by sets $\{n_{l,i}\}$ of polymer populations, where l labels the species and i labels the site. The algorithm proceeds as follows:

(1) Choose a "food set" of initial polymer populations on each site by randomly picking a fixed number (here 50) of monomers and dimers from the six available species of those lengths. (Thus, the initial distribution of food species varies from site to site.) During the simulation, if the food population becomes less than 50 on a site, randomly selected species from the six available food species types are added to bring the number to 50.

(2) At each simulation time step, sum all the intrasite chemical reaction rates possible in the lattice and denote the result $A_{\rm sum}$ where

$$A_{\rm sum} = \sum_{\rm sites} \left[\sum_{\rm ligations} v_{l,l',m,e} n_l n_{l'} n_e + \sum_{\rm scissions} v_{l,l',m,e} n_m n_e \right]. \tag{A1}$$

Denote the hopping rate per polymer by D and the total population of polymers N. Draw a random number r evenly distributed between 0 and 1. If

$$r > \frac{A_{\rm sum}}{(A_{\rm sum} + DN)}, \tag{A2}$$

then perform a diffusive hop by selecting a site and a polymer resident on it and moving this polymer to a randomly selected neighboring site. Otherwise, select an onsite reaction with a probability indicated by the master equation and adjust numbers $\{n_{l,i}\}$ to take account of the associated ligation or scission reaction, as in Ref. [4]. The real (Gillespie) time elapsed for the step is computed by drawing a random number generated from an exponential distribution with mean $A_{\rm sum} + DN$, as described in [8]. The parameter η used in the main text is related to D as $D = \frac{\eta}{1-\eta}$. For the very small η values used here, η is very close to D and may be regarded as the fixed reaction rate of diffusion per molecule.

(3) Calculate the total number of polymers on each site (N_i). If N_i exceeds a target $N_{\rm site\ max}$ (fixed at the outset to be 1000), then choose polymers at random within the site and remove them until the number is less than or equal to $N_{\rm site\ max}$.

(4) Return to (2).

As a check on the interpretation of η described in step 2, we show simulation data in which the simulated number of diffusive hops per the real (Gillespie) time as described above are plotted versus $\eta/(1-\eta)$ in Fig. 17. The relationship is linear and p-independent as expected.

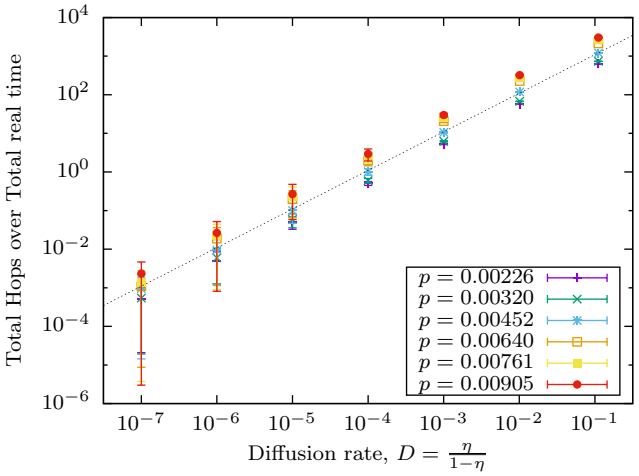

FIG. 17. Hopping rate vs the diffusion coefficient. The dotted curve is a linear function to guide the eye.

APPENDIX B: STEADY-STATE DETECTION

Because the systems considered here reached entropic steady state slowly on computational time scales, we found it convenient to implement a routine that acted "on the fly" to check when an entropic steady state was realized during simulation. This was done so that we would continue to run systems which reach steady-state entropic values slowly but could end computations early in the simulation time for states that had reached entropic steady state quickly. This saved computational resources and assured that all reported data was for systems in entropic steady state. After 10^6 simulation steps the code kept a running record of the values of $S(\{N_{L,i}\})/S_{\rm global,eq}(N)$ every ten steps over subsequent 10^5 simulation step intervals. At the end of each interval, a linear least-squares fit of those data was performed [12] and a slope estimate (β) and its error (σ_β) were calculated. If the ratio $|\beta|/\sigma_\beta < 3$, then the system was judged to be in an entropic steady state and the simulation of that realization of the model was stopped. The data from its steady-state behavior was then included in the analysis described in the text.

APPENDIX C: CONFIGURATIONAL ENTROPY

As in Ref. [4], at the most coarse-grained level, we consider the configurational entropy associated with a state described only by by the number of polymers N_L of each length L not in the food set. In the model there are 2^L possible polymer species of length L, which could be at any of the M sites. The number of microscopic states associated with this coarse-grained description is

$$W_{\rm global}(\{N_L\}) = \prod_L \sum_{\sum_i N_{L,i} = N_L} \prod_{i=1}^{M} \binom{N_{L,i} + 2^L - 1}{N_{L,i}}, \tag{C1}$$

where $N_{L,i}$ is the number of polymers of length L at site i, and we have used the binomial notation $\binom{n}{k} = \frac{n!}{k!(n-k)!}$. The binomial counts the possible species configurations of length L there could be at site i, and the product over i and the restrictive sum ($\sum_i N_{L,i} = N_L$) counts how many ways the number of polymers of length L (N_L) could be distributed over the lattice. Last, the product over L accounts for every polymer length. We derive Eq. (2) for $W_{\rm global}$ by use of the negated upper index rule for binomials [13] and a generalization of Vandermonde's

identity [14], which are, respectively,

$$\binom{n}{k} = (-1)^k \binom{k-n-1}{k}, \tag{C2}$$

$$\sum_{\sum_{j=1}^{k} i_j = m} \prod_{j=1}^{k} \binom{n_j}{i_j} = \binom{\sum_{j=1}^{k} n_j}{m}. \tag{C3}$$

Applying these identities and manipulating the expression for $W_{\text{global}}(\{N_L\})$ yields expressions containing binomials with negative upper indices. These, however, appear as ratios of the form $(-n)!/(-m)!$ and can be evaluated to give a real finite result as a limit of the ratio of Γ functions [$\lim_{z\to 0} \frac{\Gamma(z-n)}{\Gamma(z-m)} = \frac{m!}{n!}(-1)^{n-m}$, for positive integers n,m, where Γ is the Γ function]. This results is the form for W_{global},

$$W_{\text{global}}(\{N_L\}) = \prod_L \binom{N_L + M2^L - 1}{N_L}, \tag{C4}$$

establishing Eq. (2). Equation (2) can also be derived by a counting argument closely similar to the one used in Ref. [4] considering the ways of distributing N_L polymers and $2^L M - 1$ walls ($M - 1$ site walls and $2^L - 1$ species walls at every site, see also [15]). Numerical quantities computed from Eqs. (C1) and (C4) were also found to be equivalent.

[1] E. Silva and A. Lazcano, in *Molecules in Space and Time*, edited by M. Vicente, J. Tamames, A. Valencia, and J. Mingorance (Kluwer Academic, New York, 2004), pp. 13–26.

[2] T. Froese, N. Virgo, and T. Ikegami, Artif. Life **20**, 55 (2014).

[3] C. Furusawa and K. Kaneko, Artif. Life **4**, 79 (1998).

[4] A. Wynveen, I. Fedorov, and J. W. Halley, Phys. Rev. E **89**, 022725 (2014).

[5] J. Doyne Farmer, S. A. Kauffman, and N. H. Packard, Phys. D (Amsterdam, Neth.) **22**, 50 (1986).

[6] R. Bagley and J. D. Farmer, in *Artificial Life II*, edited by C. G. Langton, C. Taylor, J. D. Farmer, and S. Rasmussen (Addison-Wesley, Redwood City, CA, 1991), p. 93.

[7] S. A. Kauffman, *The Origins of Order* (Oxford University Press, New York, 1993), Chap. 7.

[8] D. T. Gillespie, J. Comput. Phys. **22**, 403 (1976).

[9] T. Tolker-Nielsen, U. C. Brinch, P. C. Ragas, J. B. Andersen, C. S. Jacobsen, and S. Molin, J. Bacteriol. **182**, 6482 (2000).

[10] A. Mendoza, S.-H. Hong, T. Osborne, M. A. Khan, K. Campbell, J. Briggs, A. Eleswarapu, L. Buquo, L. Ren, S. M. Hewitt, El.-H. Dakir, S. Garfield, R. Walker, G. Merlino, J. E. Green, K. W. Hunter, L. M. Wakefield, and C. Khanna, J. Clin. Invest. **120**, 2979 (2010).

[11] C. M. Dobson, Philos. Trans. R. Soc. London B **356**, 129 (2001).

[12] W. H. Press, S. A. Teukolsky, W. T. Vetterling, and B. P. Flannery, *Numerical Recipes in C*, 2nd ed. (Cambridge University Press, Cambridge, UK, 1996), Chap. 15.

[13] R. L. Graham, D. E. Knuth, and O. Patashnik, *Concrete Mathematics*, 2nd ed. (Addison-Wesley, Boston, 1994), Chap. 5, p. 164.

[14] This is easily proven by deriving the coefficient of x^m in the expansion of the polynomial $(1+x)^{n_1+n_2+\cdots+n_k}$.

[15] L. Landau and E. Lifshitz, in *Statistical Mechanics* (Addison-Wesley, Reading, MA, 1958), p. 116.